A Dirac Operator for Extrinsic Shape Analysis

Hsueh-Ti Derek Liu[1]   Alec Jacobson[2]   Keenan Crane[1]

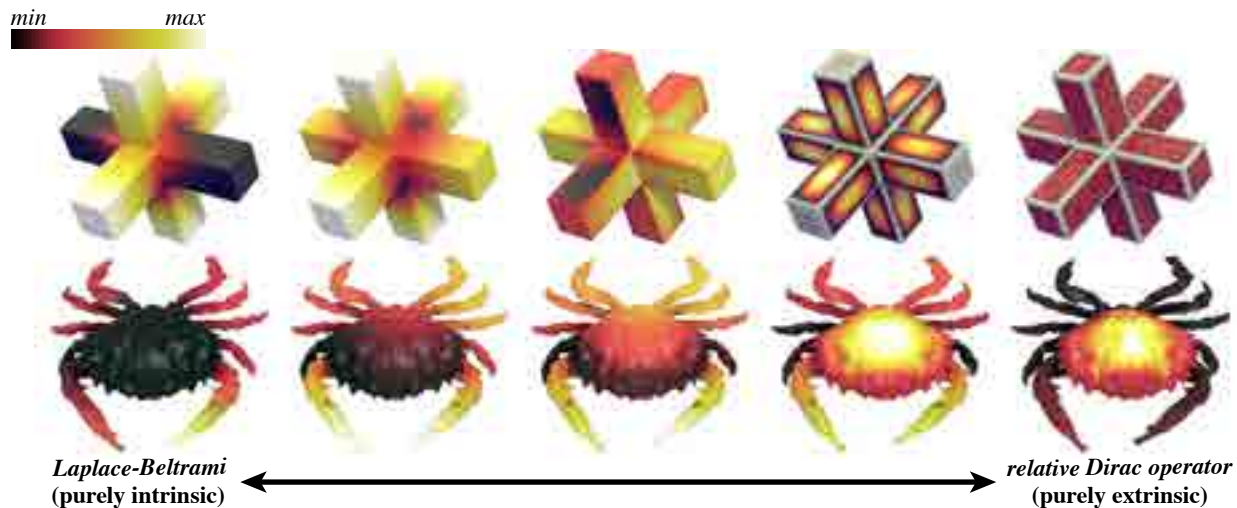[1]Carnegie Mellon University   [2]University of Toronto

Figure 1: *Not all differential operators encode the same information about shape. Here we visualize eigenfunctions of Laplace-Beltrami* (left) *which ignores extrinsic bending, and our relative Dirac operator* (right) *which ignores intrinsic stretching. In between is a continuous spectrum of operators that provide a trade off between intrinsic and extrinsic features.* Bottom: *These operators yield very different shape descriptors, here emphasizing either a pointy claw with large Gauss curvature* (left) *or the flat back of a shell with small mean curvature* (right).

Abstract

The eigenfunctions and eigenvalues of the Laplace-Beltrami operator have proven to be a powerful tool for digital geometry processing, providing a description of geometry that is essentially independent of coordinates or the choice of discretization. However, since Laplace-Beltrami is purely intrinsic it struggles to capture important phenomena such as extrinsic bending, sharp edges, and fine surface texture. We introduce a new extrinsic differential operator called the relative Dirac operator, *leading to a family of operators with a continuous trade-off between intrinsic and extrinsic features. Previous operators are either fully or partially intrinsic. In contrast, the proposed family spans the entire spectrum: from completely intrinsic (depending only on the metric) to completely extrinsic (depending only on the Gauss map). By adding an infinite potential well to this (or any) operator we can also robustly handle surface patches with irregular boundary. We explore use of these operators for a variety of shape analysis tasks, and study their performance relative to operators previously found in the geometry processing literature.*

1. Introduction

Spectral geometry processing encodes shape in terms of the eigenvalues and eigenfunctions of some (discrete) differential operator. This perspective has proven to be valuable across a wide variety of fundamental problems such as shape retrieval and surface segmentation [LZ10], providing a geometric analogue of Fourier analysis from traditional signal processing. A key feature of the spectral approach is that it allows one to easily "factor out" aspects of data that do not reflect features of the shape itself. For instance, since eigenvalues are typically rigid-motion invariant, one does not have to perform rigid alignment when comparing two shapes; likewise,

since low-frequency eigenfunctions are insensitive to discretization error, one can directly compare heterogeneous data (*e.g.*, different triangulations, or triangulations and point clouds). What other features should be factored out? In this paper we adopt the perspective that there is no one "right" answer to this question: depending on the particular application or class of objects, one might wish to put special emphasis on different geometric quantities. In particular we focus on a one-parameter family of differential operators that provides a continuous trade-off between purely *intrinsic* and *extrinsic* information (Figure 1), while preserving many of the computational benefits of existing spectral methods.

Figure 2: *A flat bed sheet, a rolled up newspaper and a canvas tent are intrinsically indistinguishable, but extrinsically distinct.*

Isometry invariance: feature or bug? On surfaces, the prototypical differential operator is the *Laplace-Beltrami operator* Δ (sometimes simply referred to as the *Laplacian*). This operator is purely *intrinsic*: it depends only on point-to-point distances *along* the surface, and not at all on how the surface sits in space (see Figure 2). Typically, isometric invariance is presented as a "feature": since the operator does not change under isometric deformation, it can be used to compare, say, human bodies in different poses, which exhibit extrinsic bending but very little intrinsic stretching (see, e.g., [RPSS10]). On the other hand, the intrinsic point of view can fail badly for other types of data—for instance, an intrinsic descriptor cannot even discriminate between the sharp edge of a cube and the flat Euclidean plane. Likewise, intrinsic measurements provide no way to detect whether a small bump on the surface points inward or outward—and yet this discrepancy can encode critical information about things like the functional behavior of proteins or pollen grains [ESP04, CW03].

One might argue that spectral data from the Laplace operator is effectively sufficient to uniquely encode shape, since it is very rare to find two "isospectral" shapes, *i.e.*, two different embeddings that induce the same metric. For instance, surfaces with positive Gaussian curvature have a unique isometric embedding, up to rigid motion [CV27]. From a practical point of view, however, the question is not simply *whether* a given operator can theoretically distinguish between two shapes, but *how big* the difference is, *e.g.*, for a small change in the surface, how *much* does the spectrum change? For applications, one may actually prefer operators that are *unstable* in this sense, since it means one can more easily discriminate between different shapes. To this end, recent alternative operators incorporate extrinsic information [HSvTP12, ARAC14], but are difficult to control: terms introduced to capture extrinsic information still do not eliminate a strong tendency to match surfaces according to their intrinsic geometry.

Contributions We introduce a family of differential operators based on the square of the *extrinsic Dirac operator* (Sec. 4), which naturally splits into an intrinsic and extrinsic part. By interpolating between these two operators we obtain a one-parameter family—at one extreme is the familiar Laplace-Beltrami operator; at the other is a novel *relative Dirac operator* which is "purely extrinsic" in the sense that it depends only on the Gauss map. The relative Dirac operator is highly sensitive to features like surface texture and sharp creases, nicely complementing existing operators that emphasize global, intrinsic features. All members of this family are self-adjoint and (weakly) elliptic, ensuring that operators come with well-defined eigenvalues and eigenbases, and making them com-

patible with standard spectral geometry processing algorithms. For partial surface analysis, we also show how to mitigate the influence of irregular boundaries by incorporating an infinite potential well. On triangle meshes we obtain a discretization by sparse matrices that agrees with the familiar *cotangent Laplacian* [Mac49] at the purely intrinsic extreme. We provide a preliminary investigation of applications in Sec. 6, showing in several cases improvement relative to existing operators.

A limitation is that our operators have a clear definition only for surfaces in $\mathbb{R}^3$, whereas some of the operators discussed in Sec. 2 can easily be defined on a manifold of any dimension.

2. Related Work

We first review differential operators on surfaces that have been used for spectral geometry processing. Why bother considering alternatives beyond Laplace-Beltrami? The basic hope is to gain additional flexibility or improved performance by swapping out an operator that captures specific geometric features of interest. A fundamental requirement is that an operator provides a well-defined and discrete (*i.e.*, enumerable) basis of eigenfunctions $(\phi_1, \phi_2, \ldots)$ and corresponding eigenvalues $(\lambda_1, \lambda_2, \ldots)$. A large number of geometry processing tasks can then be expressed in terms of (say) truncated series expansions in this basis, mirroring Fourier analysis. On a compact surface (typical of geometry processing), a discrete eigenbasis is available whenever an operator is (i) self-adjoint and (ii) elliptic. This is analogous to saying that a finite-dimensional matrix is symmetric and positive-definite. Unfortunately, many of the differential operators that arise in geometry processing (*e.g.*, the exterior derivative) do not meet these criteria. We therefore focus on just a few key examples that do, namely:

- the Laplace-Beltrami operator Δ,
- the Hessian of the *modified Dirichlet energy* [HSvTP12], and
- the *anisotropic Laplacian* Δ_A [ARAC14].

The latter two operators can distinguish between isometric shapes, but are not as sensitive to extrinsic changes as one might hope since intrinsic and extrinsic information is still "mixed together" in a way that cannot be controlled. In particular, for a surface *M* the Laplace-Beltrami operator can be viewed as the Hessian of the *Dirichlet energy* $E_D(\varphi) := \int_M |\text{grad}\varphi|^2 \, dA$ (where φ is a real-valued function on *M*); the modified Dirichlet energy re-weights the Dirichlet energy by the three components N^i of the surface normal *N*: $E_M(\varphi) := \sum_{i=1}^{3} E_D(N^i\varphi)$. The anisotropic Laplacian is defined as $\Delta_A f := \text{div}(A \, \text{grad})$, where $A : T_pM \to T_pM$ is a linear map encoding "stretching" in each tangent space T_pM; in the method of Andreux *et al.* [ARAC14] this stretching is determined by the directions and magnitudes of the (extrinsic) principal curvatures. We postpone direct comparisons with these operators until Sec. 4.1.

This paper explores the use of *Dirac operators* to enrich the landscape of tools used for spectral geometry processing. Just as Laplace-Beltrami is in a sense the most fundamental operator for real-valued functions on surfaces, *Dirac operators* are fundamental for complex (or hypercomplex) functions (Sec. 4). Our family of operators is closely linked to the *extrinsic Dirac operator* recently used to compute conformal surface deformations [CPS11], though the present work neither computes nor requires conformal maps.

What kind of applications might benefit from the use of alternative operators? For shape retrieval, *Shape DNA* [RWP06] uses the Laplace-Beltrami spectrum as a global shape descriptor; the *heat kernel signature (HKS)* [SOG09] expresses the local decay rate of heat flow via a truncated harmonic spectral expansion; and *Shape Google* [BBGO11] incorporates this descriptor into a "bag of features" approach. At each point of a surface, the values of Laplacian eigenfunctions or the heat kernel also provide an embedding of the surface into a higher-dimensional space [BBG94] which can be useful for a variety of tasks such as segmentation [WLAT14] or correspondence [Rus07]; likewise, various distance metrics are easily expressed in terms of eigenfunctions of the Laplacian or bi-Laplacian [LRF10]. The Laplacian eigenbasis also serves as the starting point for the recent *functional maps* framework [OBCS*12], which has provided leverage for a diverse range of applications [ABCCO13,ROA*13,AWO*14]. One naturally wonders how the behavior of each of these tasks changes in the presence of strong extrinsic information—a question we explore in Sec. 6.

Quaternionic signal analysis has also been used in image processing to construct Gabor filters [BS98], perform frequency domain filtering [ES07], and detect image saliency [GZ10], but does seem to appear in the shape analysis literature.

3. Background

We formulate our operators in terms of quaternion-valued differential forms. A pedagogical introduction to exterior calculus can be found in [CdGDS13]; for a detailed discussion of quaternionic forms and their relationship to geometry processing see [Cra13].

3.1. Quaternions and Surfaces

Just as the complex numbers $\mathbb{C}$ provide a convenient language for geometric operations in the plane (*e.g.*, rotations, translations, and scaling), the *quaternions* $\mathbb{H}$ provide an effective language for operations in 3D; in geometry, quaternionic analysis provides a powerful generalization of the traditional complex/Riemann surface point of view [PP98]. We will identify vectors in $\mathbb{R}^3$ with imaginary quaternions $\text{Im}\mathbb{H}$, *i.e.*, if (x,y,z) is a point in $\mathbb{R}^3$, then $x\imath + yj + zk \in \text{Im}\mathbb{H}$ is the corresponding quaternion. In this way, the geometry of a surface M can be encoded as a map $f : M \to \text{Im}\mathbb{H}$; the unit normal (or *Gauss map*) is likewise a map $N : M \to S^2 \subset \text{Im}\mathbb{H}$. A map f is an *immersion* if its derivative df is nonzero everywhere. In analogy with the complex unit $\imath$, we will use J to denote a quarter-rotation of tangent vectors in the counter-clockwise direction. To facilitate pen-and-paper calculations we will adopt the convention that f is *conformal* (*i.e.*, $df(JX) = N \times df(X)$); this convention is akin to assuming an arc-length parameterization for a curve, and (as with curves) puts absolutely no restriction on the kind of geometry we can work with in practice—in particular, we do *not* have to provide a conformal mesh parameterization. We use κ_1, κ_2 to denote the principal curvatures, and $K := \kappa_1\kappa_2$, $H := \frac{1}{2}(\kappa_1 + \kappa_2)$ to denote Gauss and mean curvature, *resp.* Finally, we use single bars $|\cdot|$ and brackets $\langle\cdot,\cdot\rangle$ to denote the norm and real inner product (*resp.*) of a finite-dimensional vector; we use double bars $||\cdot||$ and brackets $\langle\langle\cdot,\cdot\rangle\rangle$ to denote the L^2 inner product on functions, *i.e.*, $\langle\langle\phi,\psi\rangle\rangle := \int_M \phi(p)\psi(p)|df|^2$, where $|df|^2$ denotes the area element induced by f.
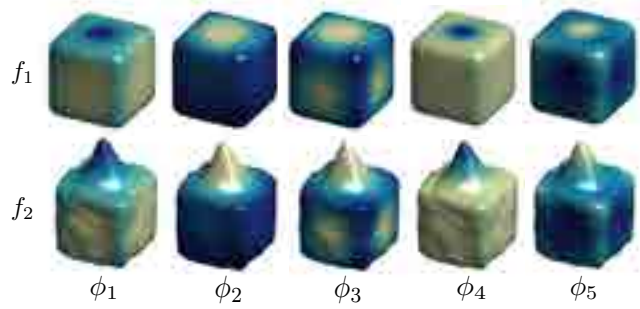

Figure 3: *The first few eigenfunctions ϕ_i of the relative Dirac operator D_{f_1,f_2}, highlighting differences between two surfaces $f_1, f_2 : M \to \mathbb{R}^3$.*

3.2. Dirac Operators

For real-valued functions on a surface, the second-order Laplace-Beltrami operator Δ is the lowest-order (nontrivial) linear differential operator that is both self-adjoint and elliptic, *i.e.*, it is in some sense the "simplest" operator with which one can hope to do spectral geometry processing. For complex (or hypercomplex) functions, however, one can find first-order differential operators that also exhibit a meaningful spectrum and eigenbasis—such operators are generally referred to as *Dirac operators*, with the most familiar example being the *Cauchy-Riemann operator* $\bar\partial$ from complex analysis. Another example is the intrinsic *Hodge-Dirac operator* $\star d + d\star$ on differential forms, recently discretized by Leopardi & Stern for problems in vector field analysis [LS14]. Because we are interested in capturing the *extrinsic* geometry of a surface, we use as a starting point the *extrinsic Dirac operator*

$$D\psi := -\frac{df \wedge d\psi}{|df|^2}.$$

where ψ is any quaternion-valued function on M, and division by $|df|^2$ corresponds to applying the 2-form Hodge star with respect to the metric induced by f [CPS11]. The basic intuition for this operator is that it generalizes the Cauchy-Riemann operator to surfaces in 3D: just as the relationship $\bar\partial\psi = 0$ characterizes conformal maps in the plane, the relationship $(D-\rho)\psi = 0$ describes a conformal surface deformation, with the new curvature determined by a real-valued function ρ. Dirac operators also naturally arise in problems from quantum mechanics and particle physics—here the quadratic form $\langle\langle D\psi,\psi\rangle\rangle$ encodes the energy level of a spin-1/2 particle (like the electron) with probability distribution $|\psi|^2$, *i.e.*, particles with "smoother" distributions have less energy. Eigenfunctions ϕ_i correspond to critical points of this energy, *i.e.*, wave functions or *spinors* describing the state of quantum spin at discrete energy levels λ_i. The wave function interpretation will be useful in formulating robust boundary conditions in Sec. 5.

4. Relative Dirac Operator

Although Dirac operators are often introduced as "square roots of the Laplacian," it is much more straightforward to see things the other way around: squaring a Dirac operator yields a Laplace-like operator. In the case of the extrinsic Dirac operator D, we get

$$D^2 \psi = \Delta \psi + \frac{dN \wedge d\psi}{|df|^2}.$$

(See [Cra13, Section 3.3].) Here Δ can be thought of as the usual (real) Laplace-Beltrami operator, acting componentwise on quaternion-valued functions. A key feature of this expression is that it cleanly separates into an intrinsic part (given by the Laplacian Δ) and an extrinsic part involving the derivative dN of the Gauss map, also known as the *shape operator*. To date, however, the latter term has not been studied as an operator in its own right. Relative to the extrinsic Dirac operator D, the only thing that changes is the appearance of dN rather than df in the numerator. In fact, many of the statements we want to make about this operator will hold not only for the Gauss map N, but for *any* pair of surfaces $f_1, f_2 : M \to \mathbb{R}^3$. Hence, we define the operator

$$D_{f_1,f_2} \psi := -\frac{df_2 \wedge d\psi}{|df_1|^2}.$$

We call this operator the *relative Dirac operator*, in reference to *relative differential geometry*, where the Gauss map N is replaced with another surface (in this case, f_2).

In practice, to evaluate this operator one must have a correspondence between the two surfaces, which in many applications is not immediately available. We will therefore mainly study the operator

$$D_N := D_{f,N} = -\frac{dN \wedge d\psi}{|df|^2}$$

associated with a single surface f, though applying the relative Dirac operator D_{f_1,f_2} in applications like shape deformation or shape differences may also prove interesting (see Figure 3 for one simple example). More generally, we consider the one-parameter family of operators obtained by interpolating between D_N and Δ:

$$L(\tau) := (1-\tau)\Delta + \tau D_N.$$

For $\tau > 0$ this family is no longer isometry invariant due to the dependence on the shape operator dN. In fact the *operator itself* is only translationally (and not rotationally) invariant, due to the
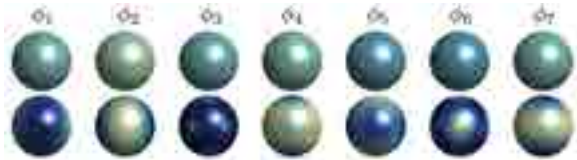

Figure 4: *Eigenfunctions on the sphere for the extrinsic part of the modified Dirichlet energy (top) and relative Dirac operator (bottom). The former becomes highly degenerate near the "extrinsic" end of the spectrum since all that remains is a 0th-order potential, whereas the latter is 1st-order and hence continues to encourage regularity in all but perfectly flat regions.*
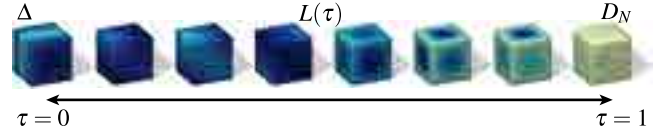

Figure 5: *On a cube, which is intrinsically flat away from corners, the Laplace operator Δ and relative Dirac operator D_N yield very different eigenfunctions. At one extreme ($\tau = 1$) every function on a flat region is an eigenfunction* (far right).

dependence on df and dN, which are expressed in an arbitrary coordinate system. Importantly, however, the *spectrum* of $L(\tau)$ remains rigid-motion invariant (App. C); the eigenfunctions are likewise canonical up to a unit constant $|q| = 1$, just as eigenfunctions of any real operator are determined only up to ± 1. In practice, this choice of unit constant causes no more (or less) trouble than in case of the Laplacian, where one must sometimes choose a canonical sign. See Sec. 4.3 for further discussion.

Figure 5 shows how this family varies for a simple cube; Figure 6 compares the behavior of Laplace, Dirac, and relative Dirac eigenfunctions on a more interesting shape. Here and throughout we plot only the pointwise *magnitude* of the eigenfunctions, though in reality each eigenfunction is a four-component quaternionic function $\phi_i : M \to \mathbb{H}$. The influence of this richer information on applications is explored in Sec. 6.

4.1. Analysis

What can we say about the behavior of the relative Dirac operator, and how does it compare with other operators in the context of spectral geometry processing? First and foremost, the relative Dirac operator will be self-adjoint and elliptic so long as both f_1 and f_2 are immersions (see Appendices A and B), making it suitable for spectral geometry processing. Notably, the operator D_N will fail to be elliptic whenever the surface f has flat regions, since here the Gauss map N fails to be an immersion. In this case, it behaves like a matrix that is only positive-*semidefinite* rather than strictly positive-definite: it has a large kernel, but is otherwise fairly well-behaved. Importantly, adding even a tiny amount of the Laplacian ($\tau < 1$) provides suitable regularization, making the operator strongly elliptic (compare two rightmost eigenfunctions in Figure 1, *(top)*). More generally, eigenfunctions of D_N will tend to have large gradients in regions of small normal curvature, since the energy $\langle\langle D_N \psi, \psi \rangle\rangle = \int_M \bar{\psi} dN \wedge d\psi$ will be small whenever the shape operator dN itself is small (see for instance Figure 1, *far right*, where the eigenfunction concentrates on the flat back of the crab). In practice, the sensitivity of the spectrum to flat regions means that the operator easily distinguishes between, say, man-made shapes (which often have many flat pieces) and organic shapes that tend to have nontrivial curvature everywhere (see Figure 9).

The behavior of other operators' eigenfunctions can also be understood in terms of curvature. For instance, the Laplace-Beltrami operator on a surface with Gauss curvature K can be expressed in local conformal coordinates as $\Delta = e^{-2u}\Delta_{\mathbb{R}^2}$, where u is the log

Figure 6: *Eigenfunctions of several operators. Both the Dirac and relative Dirac operators put more emphasis on extrinsic curvature, with the relative Dirac operator placing special emphasis on flat regions.*

conformal scale factor taking us from the surface to the plane. Since the log factor satisfies the Yamabe equation $\Delta u = K$, we see that $\Delta \varphi$ will be small in regions of large *positive* Gaussian curvature, hence eigenfunctions (which are trying to minimize $\langle\langle \Delta \varphi, \varphi \rangle\rangle$) will tend to have large gradients in such regions—see for example the crab claw in Figure 1, *far left*). The modified Dirichlet energy of Hildebrandt *et al.* [HSvTP12] can also be written as

$$E_{MDE}(\varphi) = \langle\langle \Delta \varphi, \varphi \rangle\rangle + \int_M \varphi^2 (\kappa_1^2 + \kappa_2^2) \, dA,$$

which means its Hessian is $\Delta + U$, *i.e.*, the (real) Laplace-Beltrami operator plus a Willmore potential $U := \kappa_1^2 + \kappa_2^2$ which encourages eigenfunctions to have small variation in regions where curvature is large. Here one could also develop an intrinsc-to-extrinsic family of operators, though at the "extrinsic end" it would tend toward a 0th-order operator whose eigenbasis has no clear meaning. For instance, on the unit sphere, *every* function is an eigenfunction of U (which is just a constant multiple of the identity), whereas D_N becomes the usual Dirac operator on the 2-sphere, whose eigenbasis is the standard *Dirac spinors*, akin to spherical harmonics (Figure 4). Likewise, the anisotropic Laplacian Δ_A provides a family of operators by varying the amount of anisotropy, but always retains an intrinsic component and becomes numerically unstable for large amounts of anisotropy.

4.2. Discretization

For an oriented 2-manifold triangle mesh $K = (V, E, F)$ we use a discretization of the relative Dirac operator that is identical to the one developed for the extrinsic Dirac operator [CPS11], except that we replace vertex positions f with vertex normals N when evaluating edge vectors. In particular, if $\psi : V \to \mathbb{H}$ is any piecewise linear quaternionic function, then for each triangle $ijk \in F$ the relative Dirac operator evaluates to

$$(D_N \psi)_{ijk} := -\frac{1}{2\mathcal{A}_{ijk}} \sum_{pqr \in \mathcal{C}(ijk)} (N_r - N_q) \psi_p,$$

where $\mathcal{A}_{ijk}$ is the usual triangle area and $\mathcal{C}(ijk)$ denotes the three cyclic shifts of ijk. This operator can be encoded as a matrix $D \in$
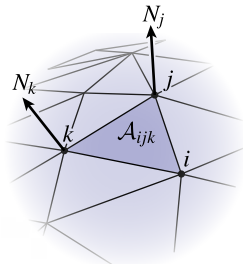
$\mathbb{H}^{|F| \times |V|}$ with nonzero entries

$$D_{ijk,p} = -(N_r - N_q)/2\mathcal{A}_{ijk}$$

for $pqr \in \mathcal{C}(ijk)$. Although this matrix is rectangular, we can accurately and efficiently compute the eigenvectors and eigenvalues using the procedure described by Crane *et al.* [CPS11, Section 5.5], using our matrix D in place of the standard Dirac operator (and letting R = 0).

4.3. Real Representation

Since most numerical linear algebra packages do not support matrices with quaternion-valued entries, we represent our matrices via 4×4 real blocks as described in [CPS11, Section 5.1]; note that the transpose of this real matrix yields the conjugate transpose of the corresponding quaternionic matrix. In this case each eigenfunction of the quaternionic operator will be represented by *four* eigenvectors of the real matrix, which differ only by an arbitrary multiplicative constant $q \in \mathbb{H}$. For spectral geometry processing applications (where we often need to compare different surfaces), it is important to choose a canonical representative. To do so, we seek the unit quaternion $|q| = 1$ that brings the entries of a given eigenvector $\phi \in \mathbb{H}^{|V|}$ as close as possible to 1; area weighting is used to avoid discrepancies in sampling. In particular, we compute

$$q := \sum_{i=1}^{|V|} \mathcal{A}_i \phi_i^{-1},$$

where $\mathcal{A}_i$ is the (barycentric) dual area associated with vertex i; we then normalize q to have unit norm before applying it to each element of ϕ. This procedure yields a canonical representative, allowing eigenfunctions on two different surfaces to be compared directly (even under a change of coordinates).

5. Boundary Conditions

For domains with boundary Bohle & Pinkall [BP13] showed that prescribing *binormal* boundary conditions preserves the self-adjointness and ellipticity of the extrinsic Dirac operator (see [CPS13, Section 6.3] for a discretization); a similar argument may be possible for the relative Dirac operator. However, the shape of the boundary can cause trouble in spectral geometry processing particularly in the case of partial matching of surface patches [RCB*17]. Rather than trying to "cut" the meshes so that they all have identical
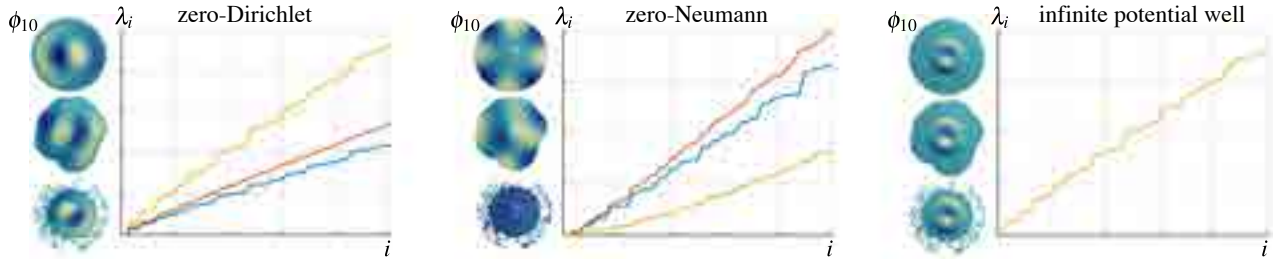
Figure 7: *Standard boundary conditions (e.g., Dirichlet or Neumann) yield spectra that are sensitive to boundary shape or discretization. By replacing such conditions with an infinite potential well, we avoid the need to consistently cut or discretize local surface patches used in partial shape matching. Here, for instance, we get consistent harmonic eigenfunctions and eigenvalues across a collection of patches with the same interior geometry, but irregular or noisy boundary.*

boundary shape, or resorting to potentially fragile re-discretization (*e.g.*, [BSK05]), we substitute standard boundary conditions for an infinite potential well that provides consistent behavior across patches with different boundary shapes or discretizations.

5.1. Infinite Potential Well

To develop our boundary treatment, we revisit the quantum mechanical interpretation: eigenfunctions of a complex differential operator L can be viewed as wave functions for a particle at different energy levels; the pointwise magnitude of this function gives the probability that a particle occupies a given region of space. This story is reflected in the fact that eigenfunctions are critical points of the energy $\langle\langle L\psi, \psi\rangle\rangle$, subject to a unit norm constraint $||\psi||^2 = \int_M |\psi|^2 \, dA = 1$ (total probability is 1). To prevent the particle from wandering near the boundary, we add a *potential U* to the operator that rapidly tends toward infinity away from the center of the domain—similar to the didactic *particle in a box* problem from quantum mechanics. Analytically, it is akin to specifying zero-Dirichlet boundary conditions on a smooth ring around the center point: minimizers of the energy $\langle\langle (\Delta + U)\psi, \psi\rangle\rangle$ must go to zero in regions where U is infinite.

Our potential is given by the modified sigmoid function

$$U(p) := \frac{c}{1 + (e^{-(d(p,q)-\beta)})^\gamma}$$

where c is a large constant, $q \in M$ is the patch center (*e.g.*, center of mass), and positive parameters , β, γ, control the diameter of the region of interest and transition width (*resp.*). For the experiments in Figure 7 we set $c = 10^{10}$, $\gamma = 100$, and use the *heat method* [CWW13] to evaluate the geodesic distance d; β is normalized such that across an entire collection of patches no boundary points are contained in the region of interest.

To incorporate this potential into real operators (*e.g.*, Laplace or anisotropic Laplace) we simply add a diagonal matrix $\mathsf{U} \in \mathbb{R}^{|V| \times |V|}$ with entries $\mathsf{U}_{ii} = \mathcal{A}_i U(p_i)$, where $\mathcal{A}_i$ and p_i are the dual area and position of vertex i, resp. For quaternionic operators (*e.g.*, Dirac or relative Dirac) which are rectangular, we build a matrix $\mathsf{B} \in \mathbb{R}^{|F| \times |V|}$ that averages vertices to faces and add the term BU to the matrix D—see Crane *et al.* [CPS11, Section 5.3] for more detail.

To verify the robustness of this scheme, we compare it to the standard Laplacian with "free" (*i.e.*, zero-Neumann) boundary condi-

tions commonly used in spectral geometry processing [LRF10], as well as simple zero-Dirichlet boundary conditions. Figure 7 plots eigenfunctions and eigenvalues for a surface patch with varying boundary shape, including noisy, nearly disconnected regions. As expected, restricting to a canonical domain through the use of a potential yields consistent spectral descriptors.

6. Applications

We take a preliminary look at using our family of operators for a variety of geometry processing tasks. Here our interest is not in exhaustively comparing against the full gamut of alternative methods, but rather in developing an understanding of how by *just changing the operator* we can augment or improve the behavior of existing *spectral* methods. In some cases (such as segmentation) this simple modification already yields results comparable to highly effective non-spectral methods [SSCO08], while providing very different algorithmic trade-offs (*e.g.*, computing eigenvectors vs. tracing rays) and operating on different types of data (*e.g.*, partial patches vs. closed meshes)—it is especially successful at identifying small extrinsic features like bumps or fingers/toes that other methods tend to miss, or diambiguating between features with similar geometry but opposite orientation.

6.1. Surface Classification

Spectral methods based on the purely intrinsic Laplace-Beltrami operator ($\tau = 0$) have proven effective for isometry-invariant surface classification (*e.g.*, ignoring bending of arms and legs in human models), but have so far been less successful at identifying high-frequency surface texture or detail. Operators at the extrinsic end of our spectrum ($\tau \to 1$) are better-suited for classifying surfaces based on such details.

Whole Surfaces. In Figure 8, we add several kinds of geometric detail to the same base torus shape, and compute the first 60 eigenvalues for several operators. Laplace-Beltrami, the anisotropic Laplacian, and the Dirac operator (which have significant intrinsic components) do a relatively poor job of distinguishing between different textures. In contrast, the modified Dirichlet energy [HSvTP12] and our relative Dirac operator clearly delineate the different surfaces, with slightly better separation in the latter case—especially if
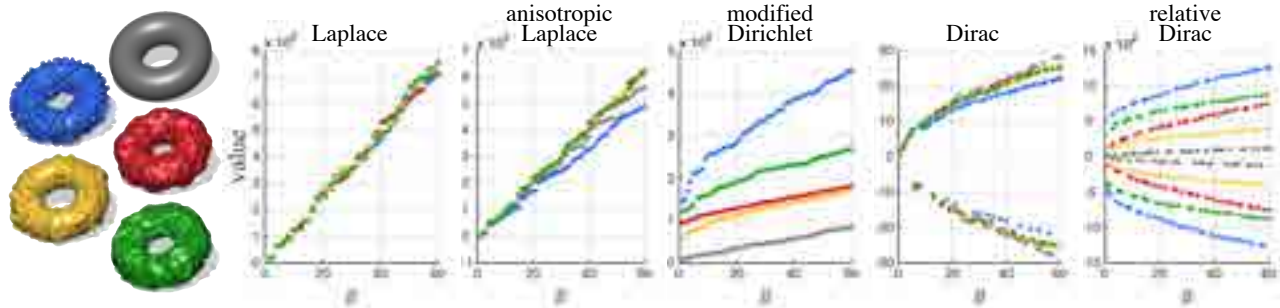
Figure 8: *The spectra of many differential operators do not clearly distinguish between surfaces with similar base shape but different fine details. The extrinsic modified Dirichlet energy performs better, though our relative Dirac operator often provides a cleaner separation (e.g., between red and yellow shapes) especially if one considers that corresponding eigenvalues often have opposite* sign, *greatly increasing the distance between spectra.*
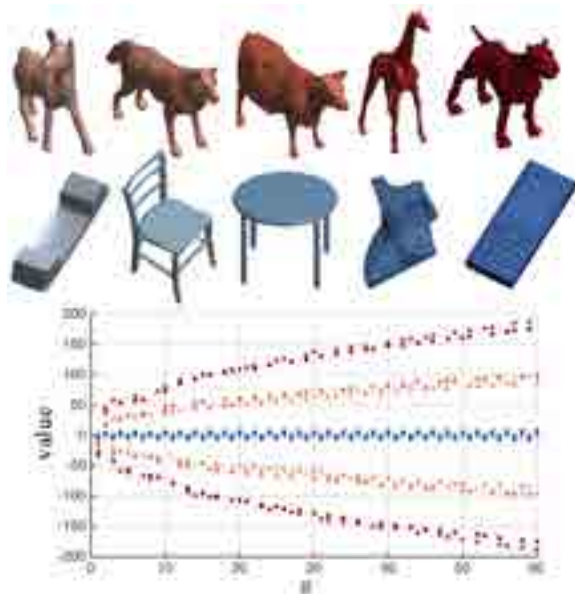

Figure 9: *Because the relative Dirac operator is sensitive to flat regions and sharp edges, it tends to provide clean separation between natural geometry (pink–red) and man-made objects (light–dark blue), which will have many small eigenvalues.*
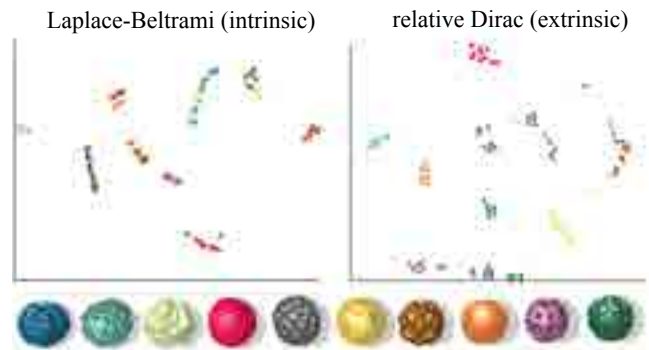

Figure 10: *Extrinsic information helps cluster surface patches according to fine texture detail. Here we visualize clusters via a low-dimensional embedding; Laplace-Beltrami (left) produces clusters that are far more "mixed" than our relative Dirac operator (right).*

one considers the fact that corresponding eigenvalues from different shapes often have opposite *sign*. This extra sign information is a unique feature of *complex* operators, providing a cleaner separation of dissimilar shapes. Figure 13 shows a similar experiment where texture covers only part of the surface.

Since our operator is particularly sensitive to flat regions, we thought it might be interesting to see how well it discriminates between man-made shapes (which tend to have flat regions) and organic shapes (which tend to have nontrivial curvature everywhere)—see Figure 9. To get a sense of performance relative to existing shape analysis tools, we labeled a subset of meshes in the SHREC dataset from [CGF09] as either "man-made" or "organic." Using a support

vector machine [CL11] based on a distribution of squared Euclidean distances (*D2* from [OFCD02]) gave a prediction accuracy of 88%, whereas averaging the square of the first 25 eigenvalues of the relative Dirac operator and thresholding at a value of 1 yielded 95% accuracy.

Surface Patches. An obvious use case for a "texture-sensitive" spectrum is to find local patches with similar texture, *à la Patch Match* [BSFG09]. Since patches extracted from an existing surface will generally have ragged, irregular boundaries, we use our infinite potential well (Sec. 5.1) to provide an "apples-to-apples" comparison between different patch spectra. To evaluate classification performance we extracted 100 surface patches from surfaces with 10 different types of texture. For a given operator, the distance between two patches is defined as the Euclidean distance between their respective spectra; this metric is then visualized in 2D using the *t-distributed stochastic neighbor embedding (t-SNE)* [MH08]. To quantify performance, we compare the average *purity* (see, *e.g.*, [MRS08], pp. 328) of 500 randomly initialized instances of k-means clustering (using the known reference value $k = 10$). Purity scores for relative Dirac,

Dirac, Laplace, anisotropic Laplace, and modified Dirichlet energy were 84.7, 76.6, 48.0, 52.7, and 61.7, respectively, with the relative Dirac operator coming closest to the ideal performance of 100.

6.2. Segmentation

Whereas eigenvalues provide a concise global shape descriptor, eigenvectors furnish useful local descriptors at each point. For a given vertex $i \in V$, a common descriptor [BBG94, Rus07] is the value of the first k eigenvectors at i, normalized by the square root of the corresponding eigenvalue:

$$v \mapsto \left(\frac{|\phi_1(v)|}{\sqrt{\lambda_1}}, \frac{|\phi_2(v)|}{\sqrt{\lambda_2}}, \frac{|\phi_3(v)|}{\sqrt{\lambda_3}}, \cdots \right).$$

Following Andreux *et al.* [ARAC14], we apply the *consensus segmentation method* [LBR*13] to this descriptor (for a variety of operators) to robustly segment surfaces—in a nutshell, the consensus method applies the idea of *persistence* to a collection of random k-means trials. We use identical parameters across all operators; the number of segments is automatically determined by the consensus algorithm (depending on how tightly vertices cluster for each operator). Figure 11 shows some examples that highlight common features: methods with a strong intrinsic component tend to produce spurious "triple points" in flattish regions where three segments meet (see for example the fish); these points are strongly reminiscent of vertices in a Voronoi diagram, and often carry no clear geometric meaning. The Dirac approach tends to avoid these spurious triple points, and also picks up on fine features like ears, toes, and the lip of the beverage pitcher.

Since there is no canonical definition for the segmentation problem, it is difficult to perform an objective quantitative comparison. To get a rough sense of performance, we ran a benchmark based on human segmentations [CGF09]. In all cases we outperformed the baseline k-means method, and achieved results moderately worse than RandCut, which was the best-performing method (scores for Human/Dirac/RandCut were 0.17/0.40/0.26, 0.07/0.19/0.13, 0.10/0.23/0.14 and 0.10/0.24/0.15 for cut discrepancy, global consistency error, Hamming distance, and rand index, respectively). Note however that we did nothing to specifically tailor our descriptor to the task of shape segmentation; a more intelligent application of the Dirac spectrum may produce better results.

6.3. Correspondence

A basic problem in shape analysis is finding a good point-to-point correspondence between a pair of shapes. One approach is to match points with a similar *heat kernel signature (HKS)*, which (roughly speaking) measures the rate of heat decay at a given point [SOG09]. For surfaces without intrinsic symmetries, the identity of a point is uniquely determined by its HKS. This descriptor can easily be generalized to any linear elliptic differential operator L by taking the diagonal part of the associated kernel, which can be approximated via the truncated series $k_t(x, y) := \sum_{i=1}^{n} e^{t\lambda_i} \phi_i(x)^2$ (where $L\phi_i = \lambda_i \phi_i$); in the case of a (hyper)complex operator one can sum over real components. By replacing the Laplace-Beltrami operator with our extrinsic Dirac operator, we obtain a new *Dirac kernel signature (DKS)* which better disambiguates between features that are extrinsically different but intrinsically similar—see Figure 12, *top* for example. (The *wave kernel signature (WKS)* [ASC11] performs similarly for this example, since it is also purely intrinsic.) Note that the improved extrinsic performance does not come at the cost of degraded overall performance—in other examples, for instance, DKS and HKS tend to have very similar performance (Figure 12, *bottom*).

7. Discussion and Limitations

Our discrete operators share many properties with the Laplacian that make it attractive for spectral geometry processing: they are sparse, easy to build, have spectra that are rigid-motion invariant, and eigenbases that can easily be put into a canonical form. Most importantly, they capture geometric features that Laplace-Beltrami cannot. However, a number of questions remain. Perhaps the most interesting question: are descriptors derived from the (relative) Dirac operator completely "informative" in the same sense as the heat kernel signature? In other words, does the Dirac kernel signature completely determine the *extrinsic* geometry (up to rigid motion)?

There are also practical issues to consider—for instance, how to best take advantage of the additional information provided by the sign of eigenvalues. For most applications we currently omit the sign, since the order of eigenvalues can be unstable with respect to perturbations of the geometry. Flat regions cause the spectrum of the relative Dirac operator to degenerate (as discussed in Sec. 4.1), an effect that is easily avoided by simply adding a small Laplacian term ($\tau < 1$). Since our operators are quaternionic (and hence must be encoded via 4×4 real blocks) their spectra are also a fair bit more expensive to compute than the conventional Laplacian, though this effect could be ameliorated via a linear algebra package that supports quaternionic data types.

Finally, there is the question of how and where extrinsic spectral analysis can benefit applications—to date spectral geometry processing has focused mainly on applications where isometry invariance is desirable (likely due to the availability of the intrinsic Laplace-Beltrami operator). Operators with strong sensitivity to extrinsic geometry clearly have the potential to complement such applications, as hinted at by the experiments in Sec. 6. A broader question is: how can application-specific geometric criteria be translated into a task-appropriate differential operator? Beyond the family of operators studied in this paper, a variety of other choices may also prove fruitful for spectral processing—for instance, the conformally invariant *Cauchy-Riemann operator*, or the *magnetic Schrödinger operator* associated with extrinsic principal curvature directions (as recently explored by Knöppel *et al.* [KCPS15]).

Figure 11: *Segmentation results using identical parameters for a variety of operators. In addition to finding strong feature curves, our extrinsic operator tends to resolve small features like ears and toes, and avoids spurious "triple points" or arbitrary patch boundaries that convey no clear geometric information (beyond an equipartition of area).*
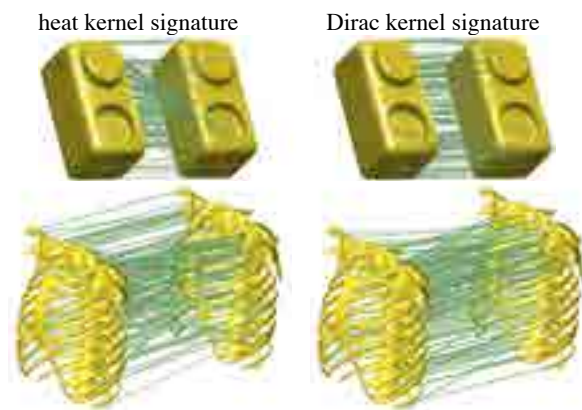
heat kernel signature   Dirac kernel signature

Figure 12: *Simple stress test: we seek point-to-point correspondence between two tessellations of the same surface. Since HKS is purely intrinsic it fails to disambiguate between "in" and "out" bump, whereas DKS yields a better match (both at bumps and in flat regions). For surfaces with strong* extrinsic *symmetry, both descriptors are equally confused.*

References

[ABCCO13] AZENCOT O., BEN-CHEN M., CHAZAL F., OVSJANIKOV M.: An Operator Approach to Tangent Vector Field Processing. *Computer Graphics Forum* (2013). 3

[ARAC14] ANDREUX M., RODOLA E., AUBRY M., CREMERS D.: Anisotropic laplace-beltrami operators for shape analysis. In *Sixth Workshop on Non-Rigid Shape Analysis and Deformable Image Alignment (NORDIA)* (2014). 2, 8

[ASC11] AUBRY M., SCHLICKEWEI U., CREMERS D.: The wave kernel signature: A quantum mechanical approach to shape analysis. In *ICCV Workshops* (2011), IEEE, pp. 1626–1633. 8

[AWO*14] AZENCOT O., WEISSMANN S., OVSJANIKOV M., WARDET-
ZKY M., BEN-CHEN M.: Functional Fluids on Surfaces. *Computer Graphics Forum* (2014). 3

[BBG94] BÉRARD P., BESSON G., GALLOT S.: Embedding Riemannian Manifolds by their Heat Kernel. *Geometric & Functional Analysis GAFA 4*, 4 (1994), 373–398. 3, 8

[BBGO11] BRONSTEIN A. M., BRONSTEIN M. M., GUIBAS L. J., OVSJANIKOV M.: Shape google: Geometric words and expressions for invariant shape retrieval. *ACM Transactions on Graphics (TOG) 30*, 1 (2011), 1. 3

[BP13] BOHLE C., PINKALL U.: Conformal deformations of immersed discs in $\mathbb{R}^3$ and elliptic boundary value problems. *arXiv preprint arXiv:1301.3752* (2013). 5

[BS98] BULOW T., SOMMER G.: Quaternionic gabor filters for local structure classification. In *Pattern Recognition, 1998. Proceedings. Fourteenth International Conference on* (1998), vol. 1, IEEE, pp. 808–810. 3

[BSFG09] BARNES C., SHECHTMAN E., FINKELSTEIN A., GOLDMAN D. B.: PatchMatch: A randomized correspondence algorithm for structural image editing. *ACM Transactions on Graphics (Proc. SIGGRAPH) 28*, 3 (Aug. 2009). 7

[BSK05] BENDELS G. H., SCHNABEL R., KLEIN R.: Detail-preserving surface inpainting. In *VAST 2005: The 6th International Symposium on Virtual Reality, Archaeology and Intelligent Cultural Heritage, Pisa, Italy, 2005* (2005), pp. 41–48. 6

[CdGDS13] CRANE K., DE GOES F., DESBRUN M., SCHRÖDER P.: Digital geometry processing with discrete exterior calculus. In *ACM SIGGRAPH 2013 courses* (New York, NY, USA, 2013), SIGGRAPH '13, ACM. 3

[CGF09] CHEN X., GOLOVINSKIY A., FUNKHOUSER T.: A benchmark for 3D mesh segmentation. *ACM Transactions on Graphics (Proc. SIGGRAPH) 28*, 3 (Aug. 2009). 7, 8

[CL11] CHANG C.-C., LIN C.-J.: Libsvm: a library for support vector machines. *ACM Transactions on Intelligent Systems and Technology (TIST) 2*, 3 (2011), 27. 7

[CPS11] CRANE K., PINKALL U., SCHRÖDER P.: Spin transformations of discrete surfaces. *ACM Trans. Graph. 30*, 4 (2011). 2, 3, 5, 6

[CPS13] CRANE K., PINKALL U., SCHRÖDER P.: Robust fairing via conformal curvature flow. *ACM Transactions on Graphics (TOG) 32*, 4 (2013), 61. 5

[Cra13] CRANE K.: *Conformal Geometry Processing*. PhD thesis, Caltech, June 2013. 3, 4, 10

[CV27] COHN-VOSSEN S.: Zwei Sätze über die Starrheit der Eiflächen. *Göttinger Nachrichten* (1927), 125–134. 2

[CW03] CHEN R., WENG Z.: A Novel Shape Complementarity Scoring Function for Protein-Protein Docking. *Proteins 51*, 3 (May 2003), 397–408. 2

[CWW13] CRANE K., WEISCHEDEL C., WARDETZKY M.: Geodesics in Heat: A New Approach to Computing Distance Based on Heat Flow. *ACM Trans. Graph. 32*, 5 (2013). 6

[ES07] ELL T. A., SANGWINE S. J.: Hypercomplex fourier transforms of color images. *IEEE Transactions on image processing 16*, 1 (2007), 22–35. 3

[ESP04] EDLUND A. F., SWANSON R., PREUSS D.: Pollen and stigma structure and function: The role of diversity in pollination. *The Plant Cell 16* (2004). 2

[GZ10] GUO C., ZHANG L.: A novel multiresolution spatiotemporal saliency detection model and its applications in image and video compression. *IEEE transactions on image processing 19*, 1 (2010), 185–198. 3

[HSvTP12] HILDEBRANDT K., SCHULZ C., VON TYCOWICZ C., POLTHIER K.: Modal shape analysis beyond laplacian. *Comput. Aided Geom. Des. 29*, 5 (June 2012), 204–218. 2, 5, 6

[KCPS15] KNÖPPEL F., CRANE K., PINKALL U., SCHRÖDER P.: Stripe patterns on surfaces. *ACM Trans. Graph. 34* (2015). 8

[LBR*13] LOURENÇO A., BULÒ S. R., REBAGLIATI N., FRED A., FIGUEIREDO M., PELILLO M.: Consensus clustering using partial evidence accumulation. In *Iberian Conference on Pattern Recognition and Image Analysis* (2013), Springer, pp. 69–78. 8

[LRF10] LIPMAN Y., RUSTAMOV R. M., FUNKHOUSER T. A.: Biharmonic distance. *ACM Trans. Graph. 29*, 3 (July 2010), 27:1–27:11. 3, 6

[LS14] LEOPARDI P., STERN A.: The abstract Hodge-Dirac operator and its stable discretization. *ArXiv e-prints* (Jan. 2014). 3

[LZ10] LEVY B., ZHANG R. H.: Spectral geometry processing. In *ACM SIGGRAPH Course Notes* (2010). 1

[Mac49] MACNEAL R.: *The Solution of Partial Differential Equations by means of Electrical Networks*. PhD thesis, Caltech, 1949. 2

[MH08] MAATEN L. V. D., HINTON G.: Visualizing data using t-sne. *Journal of Machine Learning Research 9*, Nov (2008), 2579–2605. 7

[MRS08] MANNING C. D., RAGHAVAN P., SCHÃIJTZE H.: *Introduction to Information Retrieval*. 2008. 7

[OBCS*12] OVSJANIKOV M., BEN-CHEN M., SOLOMON J., BUTSCHER A., GUIBAS L.: Functional maps: a flexible representation of maps between shapes. *ACM Transactions on Graphics (TOG) 31*, 4 (2012), 30. 3

[OFCD02] OSADA R., FUNKHOUSER T., CHAZELLE B., DOBKIN D.: Shape distributions. *ACM Transactions on Graphics (TOG) 21*, 4 (2002), 807–832. 7

[PP98] PEDIT F., PINKALL U.: Quaternionic analysis on riemann surfaces and differential geometry. *Documenta Mathematica* (1998), 389–400. 3

[RCB*17] RODOLÀ E., COSMO L., BRONSTEIN M. M., TORSELLO A., CREMERS D.: Partial functional correspondence. *Comput. Graph. Forum 36*, 1 (2017), 222–236. 5

[ROA*13] RUSTAMOV R. M., OVSJANIKOV M., AZENCOT O., BEN-CHEN M., CHAZAL F., GUIBAS L. J.: Map-based exploration of intrinsic shape differences and variability. *ACM Trans. Graph. 32*, 4 (2013), 72:1–72:12. 3

[RPSS10] RUGGERI M. R., PATANÈ G., SPAGNUOLO M., SAUPE D.: Spectral-driven isometry-invariant matching of 3d shapes. *Int. J. Comput. Vision 89*, 2-3 (Sept. 2010), 248–265. 2

[Rus07] RUSTAMOV R. M.: Laplace-beltrami eigenfunctions for deformation invariant shape representation. In *Symposium on Geometry Processing* (Aire-la-Ville, Switzerland, Switzerland, 2007), SGP '07, Eurographics Association, pp. 225–233. 3, 8

[RWP06] REUTER M., WOLTER F.-E., PEINECKE N.: Laplace–beltrami spectra as 'shape-dna' of surfaces and solids. *Computer-Aided Design 38*, 4 (2006), 342–366. 3

[SOG09] SUN J., OVSJANIKOV M., GUIBAS L.: A concise and provably informative multi-scale signature based on heat diffusion. In *Computer graphics forum* (2009), vol. 28, Wiley Online Library, pp. 1383–1392. 3, 8

[SSCO08] SHAPIRA L., SHAMIR A., COHEN-OR D.: Consistent mesh partitioning and skeletonisation using the shape diameter function. *The Visual Computer 24*, 4 (2008), 249–259. 6

[WLAT14] WANG H., LU T., AU O. K.-C., TAI C.-L.: Spectral 3d mesh segmentation with a novel single segmentation field. *Graphical models 76*, 5 (2014), 440–456. 3

Appendix: Properties of the Relative Dirac Operator

In the discrete case, any Hermitian matrix has orthogonal eigenvectors and real eigenvalues. This fact is of course not sufficient to guarantee that the original continuous operator discretized by such a matrix has a well-defined spectral decomposition. To ensure that spectral analysis carried out via our new operator is actually meaningful (*i.e.*, it is not highly mesh-dependent and has a meaningful limit under refinement), we show here that the relative Dirac operator D_{f_1,f_2} is self-adjoint and (weakly) elliptic, which is sufficient to ensure that it has a real, discrete spectrum of eigenvalues, and corresponding orthonormal basis of eigenfunctions. This kind of consistency is especially important for ensuring that one does not get unpredictable behavior for different tessellations of the same surface. These arguments are mild modifications of those found in [Cra13, Section 3.1]. We also show that the spectrum is rigid motion invariant, and that the eigenfunctions are covariant with respect to rotation. These properties ensure that spectral data can be compared across surfaces expressed in different coordinate frames.

Appendix A: Self-Adjointness

A linear operator A is *self-adjoint* if $\langle\langle A\psi, \phi\rangle\rangle = \langle\langle\psi, A\phi\rangle\rangle$ for all pairs of functions ψ, ϕ. Consider any two functions $\phi, \psi : M \to \mathbb{H}$. Then

$$\langle\langle\psi, D_{f_1,f_2}\rangle\rangle = -\int_M \bar\psi \frac{df_2 \wedge d\phi}{|df_1|^2} |df_1|^2 = \int_M \bar\psi df_2 \wedge d\phi$$
$$= \int_M d\bar\psi \wedge df_2\phi - \int_M d(\bar\psi df_2\phi).$$

On closed surfaces the latter term vanishes (by Stokes' theorem) and we are left with just

$$\int_M d\bar\psi \wedge df_2\phi = -\int_M \overline{\bar\phi dN \wedge d\psi} = \overline{\langle\langle\phi, D_{f_1,f_2}\psi\rangle\rangle} = \langle\langle D_{f_1,f_2}\psi, \phi\rangle\rangle,$$

as desired.

Appendix B: Ellipticity

For any immersion f we can pick local coordinates s_1, s_2 on M to get

$$df \wedge d\psi = \left(\frac{\partial f}{\partial s_1}ds^1 + \frac{\partial f}{\partial s_2}ds^2\right) \wedge \left(\frac{\partial\psi}{\partial s_1}ds^1 + \frac{\partial\psi}{\partial s_2}ds^2\right)$$
$$= \left(\frac{f}{s_1}\frac{\psi}{s_2} - \frac{f}{s_2}\frac{\psi}{s_1}\right)ds^1 \wedge ds^2.$$

Letting $f = f_2$, this means that

$$-D_{f_1,f_2}\psi = \frac{df_2 \wedge d\psi}{|df_1|^2} = \underbrace{\frac{|df_2|^2}{|df_1|^2}}_{=:K_{f_1,f_2}} \frac{df_2 \wedge d\psi}{|df_2|^2} = K_{f_1,f_2}\left(\frac{\partial f_2}{\partial s_2}\frac{\partial \psi}{\partial s_1} - \frac{\partial f_2}{\partial s_1}\frac{\partial \psi}{\partial s_2}\right).$$

We will refer to K_{f_1,f_2} as the *relative Gaussian curvature*, since it corresponds to the standard Gaussian curvature whenever $f_1 = f$ and $f_2 = N$. The symbol of D_{f_1,f_2} is then the linear map

$$p(s_1,s_2) := K_{f_1,f_2}\left(\frac{\partial f_2}{\partial s_2}s_1 - \frac{\partial f_2}{\partial s_1}s_2\right),$$

which we can also write as

$$p(X) = K_{f_1,f_2}df_2(JX)$$

for any vector $X := (s_1, s_2)$, and J is the complex structure induced by f_2. The relative Dirac operator is then (weakly) elliptic whenever the symbol p is nondegenerate, *i.e.*, whenever both f_1 and f_2 are immersions. In particular, in order for $D_{f,N}$ to be elliptic it is insufficient for the surface to merely have no flat regions—it must also not have any *developable* regions ($K = 0$), in which case dN will vanish along (at least) the minimum principal direction. In fact, the only surfaces for which $D_{f,N}$ is everywhere weakly elliptic are those which are strictly convex, since on surfaces with both positive and negative curvature, K must vanish somewhere. As discussed in Sec. 4.1, however, the operator still behaves reasonably in practice, especially for any value $\tau < 1$, *i.e.*, adding even a tiny amount of Laplace-Beltrami makes the operator strongly elliptic.

Appendix C: Rigid Motion Invariance of Spectral Data

We here examine the behavior under rigid motion of the eigenvalues and eigenfunctions of the extrinsic Dirac operator $D_f\psi := \frac{df \wedge d\psi}{|df|^2}$. The spectrum of the relative Dirac operator behaves the same way, since the surface normal N obeys the same transformation law as the differential df, *i.e.*, $\tilde{N} = q^{-1}Nq$.

Proposition 1 For any $q \in \mathbb{H}$,

$$D_f(q\psi) = qD_{\tilde{f}}\psi,$$

where $d\tilde{f} = q^{-1}dfq$, *i.e.*, the two differentials are related by a rotation (so that the immersions themselves are related by rotation and translation).

Proof We have

$$D_f(q\psi) = \frac{df \wedge d(q\psi)}{|df|^2} = \frac{(df)q \wedge d\psi}{|df|^2},$$

and hence

$$q^{-1}D_f(q\psi) = \frac{(q^{-1}df\,q) \wedge d\psi}{|q^{-1}df\,q|^2} = \frac{d\tilde{f} \wedge d\psi}{|d\tilde{f}|^2} = D_{\tilde{f}}\psi,$$

as desired. $\quad\square$

Proposition 2 Eigenvalues of D_f are invariant with respect to rigid motions; eigenfunctions are covariant with respect to rotation (and invariant with respect to translation).
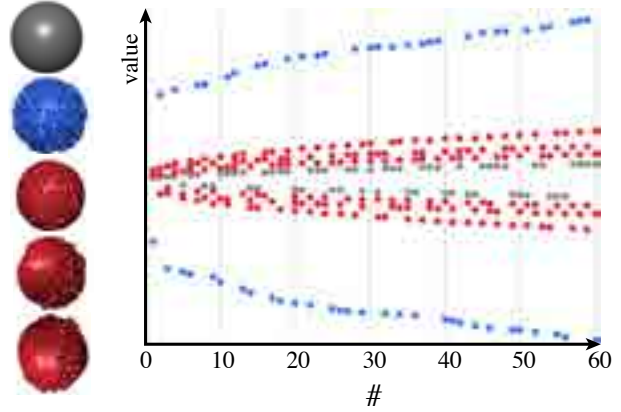

Figure 13: *The relative Dirac operator successfully discriminates between texture that covers the entire surface (blue), and surfaces partially covered by the same texture (red).*

Proof For any eigenfunction ϕ of $D_{\tilde{f}}$ with associated eigenvalue λ, we can apply Proposition 1 to get

$$\begin{array}{rcl} D_{\tilde{f}}\phi &=& \lambda\phi \\ \Longleftrightarrow \quad q^{-1}D_f(q\phi) &=& \lambda\phi \\ \Longleftrightarrow \quad D_f(q\phi) &=& \lambda q\phi, \end{array}$$

i.e., D_f has the same eigenvalues as $D_{\tilde{f}}$, and the same eigenvectors up to the constant q. $\quad\square$